

Acoustic Superradiance from a Bose-Einstein Condensate Vortex with a Self-Consistent Background Density Profile

Betül Demirkaya*, Tekin Dereli†, Kaan Güven‡

Department of Physics, Koç University, 34450 Sarıyer, İstanbul, Turkey

December 16, 2021

Abstract

The axisymmetric acoustic perturbations in the velocity potential of a Bose-Einstein condensate in the presence of a single vortex behave like minimally coupled massless scalar fields propagating in a curved (1+1) dimensional Lorentzian space-time, governed by the Klein-Gordon wave equation. Thus far, the amplified scattering of these perturbations from the vortex, as a manifestation of the acoustic superradiance, has been investigated with a constant background density. This paper goes beyond by employing a self-consistent condensate density profile that is obtained by solving the Gross-Pitaevskii equation for an unbound BEC. Consequently, the loci of the event horizon and the ergosphere of the acoustic black hole are modified according to the radially varying speed of sound. The superradiance is investigated both for transient features in the time-domain and for spectral features in the frequency domain. In particular, an effective energy-potential function defined in the spectral formulation correlates with the existence and the frequency dependence of the acoustic superradiance. The numerical results indicate that the constant background density approximation underestimates the maximum superradiance and the frequency at which this maximum occurs.

*bdemirkaya@ku.edu.tr

†tdereli@ku.edu.tr

‡kguven@ku.edu.tr

1 Introduction

Unruh introduced the idea of condensed-matter analogies of gravitational systems by showing that acoustic perturbations in the velocity potential of a locally irrotational, barotropic, inviscid Newtonian fluid behave exactly as a minimally coupled massless scalar fields propagating in a curved $(3 + 1)$ dimensional Lorentzian spacetime [1]. Since then, different condensed-matter and optical systems have been studied to demonstrate the analogies of various cosmic-scale gravitational phenomena down at the laboratory scale. [2]. In the last few years, experimental realizations of black- and white-horizons were reported in water channels [3], atomic Bose-Einstein condensates (BECs) [4], nonlinear optical fibers and silica glass illuminated by strong laser pulses, and also in nonlinear optical systems [5],[6]. In 2014, Acoustic black hole in a needle-shaped BEC of 87Rb is achieved and recently spontaneous Hawking radiation, stimulated by quantum vacuum fluctuations, emanating from an analogue black hole in an atomic Bose-Einstein condensate is reported [7],[8].

One of the striking features of rotating atomic BECs is the formation of vortices [9]. The occurrence of vortices in superfluids has been the focus of fundamental theoretical and experimental works [10], [11], [12]. Scattering process from a single vortex, the superradiance phenomena, has been analyzed theoretically and numerically for constant density approximation in BECs as well as in classical fluid [13], [14].

Motivated by the recent experimental progress in BEC systems, we present here a consolidating study of the temporal and spectral features of the scattering process from a BEC vortex with non-constant background density with a modified version of the Visser's draining bathtub model (DBT) [15]. Constant density, therefore constant speed of sound approximation provide certain freedom in choosing the fluid velocity and the scaling factor. However, for a single unbound vortex in BEC, rotational velocity is naturally quantized [cite] and the radial velocity is shaped by the continuity equation with the defined density profile, which shapes the speed of sound throughout the vortex. Since velocities and density are linked together, we loose the freedom to increase the vortex fluid without changing the profiles for density and the speed of sound. However, for a stable single vortex these assumptions are physically more plausible.

In this paper we analyzed the two main assumptions constant and non-constant density assumptions, and compare the result within the superradiance calculations. Single unbound vortex density is calculated via the Gross-Pitaevskii equation which gives a density profile that sets the non-constant speed of sound with a natural scaling factor, healing length. The time domain solutions are obtained by solving the Klein-Gordon equation for the propagation of acoustic waves by implementing the numerical techniques described mainly in Ref.s [16],[17],[18], whereas the spectral analysis of the superradiance is conducted by asymptotic solutions of the waves at the event horizon and the ergosphere. In addition wave equation in frequency domain is solved, numerically, to calculate the reflection coefficient after the coordinate transformation in order to avoid the singularity, event horizon.

2 The vortex state of an unbound BEC condensate

The single vortex state in the condensate of weakly interacting bosons is described by the Gross-Pitaevskii (GP) equation,

$$i\hbar \frac{\partial \Psi}{\partial t} = \left(-\frac{\hbar^2}{2m} \nabla^2 + V_{ext} + U_0 |\Psi|^2 \right) \Psi(r, t) \quad (2.1)$$

where V_{ext} is the external potential and $V_H = \frac{4a\pi\hbar^2}{m} |\Psi|^2 \equiv U_0 |\Psi|^2$ is the repulsive Hartree potential for binary interactions among atoms, that is characterized by the scattering length, a , V_H prevents the collapse instability.

For an unbounded condensate (i.e $V_{ext} = 0$), on dimensional grounds, the balance between the kinetic energy and V_H implies a correlation(healing) length

$$\xi^2 = \frac{\hbar^2}{2\rho_\infty m U_0} = \frac{1}{8\pi\rho_\infty a} \quad (2.2)$$

ρ_∞ donates the bulk density of the uniform condensate. The healing length describes the distance at which the condensate wave function tends to its bulk form in the presence of localized perturbations [10],[19].

The stationary solutions take the form $\Psi(r, t) = \psi(r)e^{-i\mu t/\hbar}$ with a background density $\rho(r) = |\psi(r)|^2$ and chemical potential $\mu = \frac{\hbar^2}{2m\xi^2}$. For a vortex state, the radial part has a axisymmetric formal solution in polar coordinates

$$\psi(r, \theta) = f_q(r)e^{iq\theta}, \quad (2.3)$$

where the subscript q donates the winding number. Substituting Eq.2.3 into Eq.2.1 yields

$$\mu\psi(r) = -\frac{\hbar^2}{2m} \frac{1}{r} \frac{\partial}{\partial r} \left(r \frac{\partial f_q}{\partial r} \right) + \frac{\hbar^2}{2mr^2} f_q + U_0 f_q^3. \quad (2.4)$$

Using dimensionless radial coordinate $\tilde{r} = r/\xi$ and the scaled function $\chi_q = f_q/\sqrt{\rho_\infty}$ the equation takes the form

$$\frac{1}{\tilde{r}} \frac{d}{d\tilde{r}} \left(\tilde{r} \frac{d\chi_q}{d\tilde{r}} \right) + \frac{\chi_q}{\tilde{r}^2} + \chi_q^3 - \chi_q = 0. \quad (2.5)$$

Subject to the boundary conditions

$$\chi_q(0) = 0 \quad \chi_q(\infty) = 1. \quad (2.6)$$

The vortices with respective winding numbers $q = \pm 1$ are found to be topologically stable but that those with larger values of $|q|$ are unstable and should decay into $|q| = 1$ single-charge vortices [20], [21]. Thus, Eq.2.5 is solved for $q = 1$ only. Although a closed analytical form of solution is not available, an approximate functional form is given by [19],[22]

$$\chi_1 = \sqrt{\frac{\tilde{r}^2}{2 + \tilde{r}^2}}, \quad (2.7)$$

which provides a good approximation to the numerical solution as shown in Fig.1. In the next section, the approximate form will be employed to proceed with the theoretical formulation, but the full solution will be used for obtaining the numerical results.

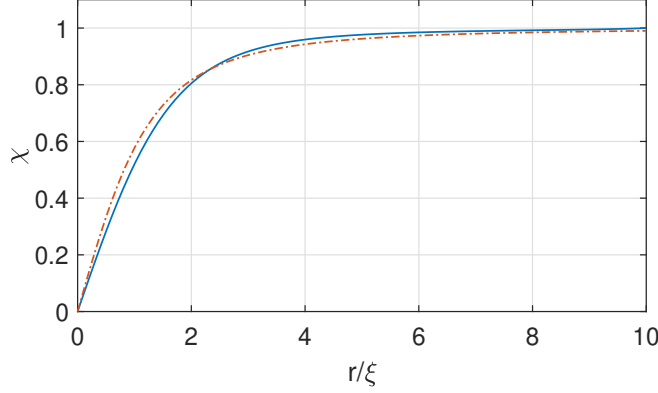


Figure 1: The radial wave function $\chi(r/\xi)$ obtained by numerical solution of the stationary GP equation for a straight vortex line with the approximate form given in Eq.2.7 shown by a dashed line.

2.1 Dynamics of the vortex

The definition of velocity in BEC is irrotational, which is a typical characteristic of superfluids [10]. However, in the presence of a vortex, the velocity is singular at the vortex center and the circulation around a contour enclosing the vortex becomes nonzero. Hence, the velocity acquires a tangential component, described by a winding number

$$\Theta = \oint \vec{v} \cdot d\vec{l} = 2\pi q \frac{\hbar}{m}, \quad q = \pm 1, \pm 2, \dots \quad (2.8)$$

$$v_{\hat{\theta}} = \frac{\Theta}{2\pi r} \hat{\theta}. \quad (2.9)$$

In order to satisfy the continuity equation in cylindrical coordinates $\frac{\partial \rho}{\partial t} + \nabla \cdot (\rho \vec{v}) = 0$, the radial component of the velocity becomes

$$\nabla \cdot (\rho_0 \vec{v}) = 0 \Rightarrow v_{\hat{r}} = -\frac{A}{\rho(r)r} \quad (2.10)$$

Hence, the draining bathtub model described in Ref.s [23],[24] has to be modified accordingly:

$$\vec{v} = \frac{-A}{r} \hat{r} + \frac{B}{r} \hat{\phi} \rightarrow \vec{v} = \frac{-A}{\rho(r)r} \hat{r} + \frac{B}{r} \hat{\phi}. \quad (2.11)$$

The parameters A and B are described in the next section.

3 Solution to Klein-Gordon equation in time domain

With the radially varying background density profile, the GP equation can now be solved for first order fluctuations $\psi = \psi_0 + \psi_1 = \sqrt{\rho}e^{i\Phi}$, against the background $\psi_0 = \sqrt{\rho_0}e^{i\Phi_0}$. This yields a set of two equations. The first one is the continuity equation

$$\frac{\partial \rho}{\partial t} + \nabla \cdot (\rho \vec{v}) = 0 \quad (3.1)$$

and the so-called Euler equation with an additional term (first term on right-hand side of Eq.3.2) which is called the quantum pressure.

$$\partial_t \vec{v} + (\vec{v} \cdot \vec{\nabla}) \vec{v} = \frac{\hbar^2}{2m^2} \nabla \left(\frac{1}{\sqrt{\rho}} \nabla^2 \sqrt{\rho} \right) - \frac{\nabla V_{ext}}{m} - \frac{\nabla (U_0 \rho)}{m}. \quad (3.2)$$

Eq.s 3.1 and 3.2 are expressed in terms of the velocity of the condensate defined as

$$\vec{v} = (\hbar/m) \nabla \Phi. \quad (3.3)$$

The dynamics of small fluctuations can be formulated by linearizing the equations against the background: $\rho = \rho_0 + \rho_1$, $\Phi = \Phi_0 + \Phi_1$. This yields the equation system

$$\frac{\partial \rho_0}{\partial t} + \nabla \cdot (\rho_0 \vec{v}) = 0 \quad (3.4)$$

$$\partial_t \Phi_0 = \frac{|\nabla \Phi_0|^2}{2m^2} + \frac{V_{ext}}{m} + \frac{U_0 \rho_0}{m} - \frac{\hbar^2}{2m} \frac{\nabla^2 \sqrt{\rho_0}}{\sqrt{\rho_0}} \quad (3.5)$$

$$\frac{\partial \rho_1}{\partial t} + \frac{\hbar}{m} \nabla \cdot (\rho_0 \nabla \Phi_1) + \nabla \cdot (\rho_1 \vec{v}) = 0, \quad (3.6)$$

$$\partial_t \Phi_1 = -v \cdot \nabla \Phi_1 - \frac{U_0}{\hbar} \rho_1 + \frac{\hbar^2}{2m} D_2 \rho_1, \quad (3.7)$$

where D_2 is

$$D_2 = \frac{1}{2\sqrt{\rho_0}} \nabla^2 \frac{\rho_1}{\sqrt{\rho_0}} - \frac{\rho_1}{2\rho_0^{3/2}} \nabla^2 \sqrt{\rho_0}. \quad (3.8)$$

Note that Eq.s 3.4-3.5 indicate that the background satisfies itself the GP equation whereas Eq.s 3.6-3.7 govern the fluctuation dynamics. For small fluctuations, D_2 is negligible in comparison to other terms [19]. This establishes the hydrodynamic (quasi-classical) approximation, under which Eq.s 3.6 and 3.7 are combined to yield a single equation for the phase fluctuations

$$\frac{\partial}{\partial t} \left[\frac{\rho_0}{c^2} \left(\frac{\partial \Phi_1}{\partial t} + \vec{v} \cdot \nabla \Phi_1 \right) \right] - \nabla \cdot (\rho_0 \nabla \Phi_1) + \nabla \cdot \left[\frac{\rho_0}{c^2} \left(\frac{\partial \Phi_1}{\partial t} + \vec{v} \cdot \nabla \Phi_1 \right) \right] = 0. \quad (3.9)$$

Now, the background density profile can be introduced by the approximate functional form for a single vortex state through Eq.2.7 with $\rho(r) = |\psi(r, \theta)|^2$ resulting in

$$\rho_0(r) = \rho_\infty \frac{(r - r_0)^2}{(r - r_0)^2 + 2\xi^2} \quad (3.10)$$

where r_0 is the vortex center, ξ is the healing length and $\rho_\infty = \frac{1}{8\pi\xi^2 a}$ is the bulk density far away from the vortex. The propagation speed of sound in a BEC is given by $c = \sqrt{U_0 \rho / m}$ which becomes a radially varying function near the vortex:

$$c(r) = c_\infty \sqrt{\frac{(r - r_0)^2}{(r - r_0)^2 + 2\xi^2}}, \quad (3.11)$$

where $c_\infty = \frac{\hbar}{m} \sqrt{4\pi a \rho_\infty}$ denotes the bulk value for sound speed. Taking $r_0 = 0$ and using cylindrical coordinates, Eq.3.9 can be written in explicit form as

$$\begin{aligned} & \left[\frac{\partial^2}{\partial t^2} + 2v_r \frac{\partial^2}{\partial t \partial r} + \frac{2v_\theta}{r} \frac{\partial^2}{\partial t \partial \theta} + (-c^2 + v_r^2) \frac{\partial^2}{\partial r^2} + \frac{2v_\theta v_r}{r} \frac{\partial^2}{\partial r \partial \theta} \right. \\ & + \left(-\frac{c^2}{r^2} + \frac{v_\theta^2}{r^2} \right) \frac{\partial^2}{\partial \theta^2} + \frac{1}{r} \frac{\partial(rv_r)}{\partial r} \frac{\partial}{\partial t} + \left(-\frac{v_\theta v_r}{r^2} + \frac{v_\theta}{r} \frac{\partial v_r}{\partial r} \right) \frac{\partial}{\partial \theta} \\ & \left. + \left(-\frac{c^2}{r} - \frac{c^2}{\rho} \frac{\partial \rho(r)}{\partial r} + \frac{v^2}{r} + 2v_r \frac{\partial v_r}{\partial r} + v_\theta \frac{\partial v_\theta}{\partial r} \right) \frac{\partial}{\partial r} - c^2 \frac{\partial^2}{\partial z^2} \right] \Phi_1 = 0. \quad (3.12) \end{aligned}$$

In the following, the numerical techniques described in Ref.s [16],[17] are being implemented (the Φ_1 of the present formulation corresponds to Ψ in these references). Two conjugate fields are introduced:

$$\Gamma = \frac{\partial \Phi}{\partial x^i} \quad \Pi = -\frac{1}{c} \left(\frac{\partial \Phi}{\partial t} - \beta^i \Gamma_i \right), \quad (3.13)$$

where $x_i = (r, \theta, z)$ denote the cylindrical coordinates and $\beta^i = (-v_r, -v_\theta/r, 0)$ are the velocity components. The fields are introduced formally as

$$\Phi = \phi_1(t, r) e^{im\phi} e^{ikz} \quad \Pi = \pi_1(t, r) e^{im\phi} e^{ikz} \quad \Gamma = \gamma_1(t, r) e^{im\phi} e^{ikz} \quad (3.14)$$

with (k, m) denoting the axial and azimuthal wave numbers. In this study, we take $k = 0$, i.e. translational symmetry along the z axis. These functional forms satisfy a set of first order coupled partial differential equations

$$\frac{\partial \phi_1}{\partial t} = -c\pi_1 - v_r \gamma_1 - \frac{imv_\theta}{r} \phi_1 \quad (3.15)$$

$$\begin{aligned}\frac{\partial \gamma_1}{\partial t} = & -\frac{\partial c}{\partial r} \pi_1 - c \frac{\partial \pi_1}{\partial r} - \frac{\partial v_r}{\partial r} \gamma_1 - v_r \frac{\partial \gamma_1}{\partial r} \\ & - \frac{\partial v_\theta}{\partial r} \frac{im}{r} \phi_1 + \frac{im v_\theta}{r^2} \phi_1 - \frac{im v_\theta}{r} \frac{\partial \phi_1}{\partial r}\end{aligned}\quad (3.16)$$

$$\begin{aligned}\frac{\partial \pi_1}{\partial t} = & \pi_1 \left(-\frac{\partial c}{\partial r} \frac{v_r}{c} - \frac{im v_\theta}{r} - \frac{1}{r} \frac{\partial (r v_r)}{\partial r} \right) - v_r \frac{\partial \pi_1}{\partial r} \\ & + \frac{\gamma_1}{c} \left(-\frac{c^2}{r} - \frac{c^2}{\rho} \frac{\partial \rho}{\partial r} + \frac{v_\theta^2}{r} + v_\theta \frac{\partial v_\theta}{\partial r} \right) - c \frac{\partial \gamma_1}{\partial r} \\ & + \frac{\phi_1}{c} \left(\frac{m^2 c^2}{r^2} + c^2 k^2 - \frac{im v_r}{r} \frac{\partial v_\theta}{\partial r} - \frac{im v_r v_\theta}{r^2} \right)\end{aligned}\quad (3.17)$$

In section 4, the superradiance will be investigated through the propagation of these conjugate fields by solving these equations numerically.

3.1 The Event Horizon and the Ergosphere

The vortex state defines a curved 1+1 space-time where the line element reads

$$ds^2 = \frac{\rho}{c} [-cdt^2 + (dr - v_r dt)^2 + (rd\theta - v_\theta dt)^2]. \quad (3.18)$$

A new coordinate system is introduced through the following transformations that minimize the number of off-diagonal elements in the metric, thereby revealing the event horizon and the ergosphere.

$$dt = dt^* - v_r / (c^2 - v_r^2) dr, \quad (3.19)$$

$$d\theta = d\theta^* - v_r v_\theta / (r (c^2 - v_r^2)) dr, \quad (3.20)$$

$$r = r^*, z = z^*, \quad (3.21)$$

For simplicity, the new coordinates are renamed as the old ones from now on. The line element takes the form

$$ds^2 = \left[(v^2 - c^2) dt^2 + \frac{c^2}{c^2 - v_r^2} dr^2 + r^2 d\theta^2 + 2v_\theta r dt d\phi \right]. \quad (3.22)$$

In general relativity, the radius of the ergosphere, r_e , for a Kerr-type black hole is defined through the vanishing of the coefficient of dt^2 , whereas the event horizon, r_h , is determined by the singularity of the metric. These conditions read respectively as

$$v^2 - c^2 = 0 \Rightarrow \frac{A}{\rho_\infty c_\infty} - \frac{r_h^4}{(r_h^2 + 2\xi^2)^{3/2}} = 0 \quad (3.23)$$

$$v_r^2 - c^2 = 0 \Rightarrow \frac{A^2 (r_e^2 + 2\xi^2)^2}{\rho_\infty^2 r_e^6} + \frac{B^2}{r_e^2} - \frac{c_\infty^2 r_e^2}{r_e^2 + 2\xi^2} = 0 \quad (3.24)$$

The coefficients A and B can be chosen to set the event horizon at unit healing length $r_h = \xi$:

$$A = \frac{\xi \rho_\infty c_\infty}{3^{3/2}} \quad B = \frac{\hbar}{m}. \quad (3.25)$$

Note that B follows from Eq.2.9. As a practical example, we employ the parameters of a BEC of Rb-87 atoms taken from Ref.s[25],[26]:

$$a = 5.77 \text{ nm} \quad m = 1.44 * 10^{-25} \text{ kg} \quad \rho_\infty = 10^{21} \text{ m}^{-3} \quad (3.26)$$

which yields

$$c_\infty = 6.2 * 10^{-3} \text{ m/s} \quad \xi = 83 \text{ nm} \quad (3.27)$$

By substituting these values into Eq.3.24, the resulting polynomial of degree 8 in r_e can be solved numerically, which has only one positive real root: $r_e = 1.84\xi$. Figure 2 shows the event horizon, the ergosphere along with the variation of the speed of sound and the radial velocity of the condensate fluid near the vortex.

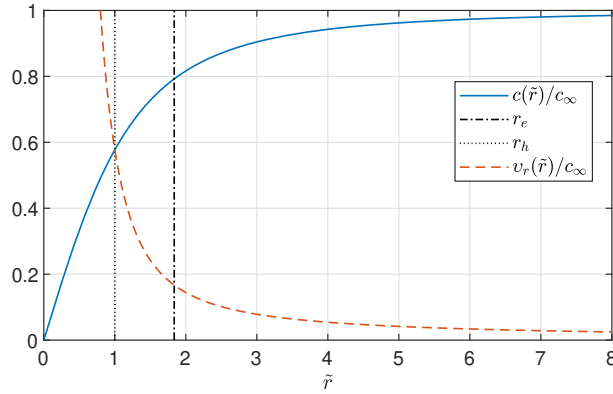


Figure 2: Representation of the event horizon, r_h , ergoregion, r_e , the speed of sound, $c(r)$ and the radial velocity of the fluid, $v_r(r)$ near vortex.

4 Acoustic superradiance in the time-domain

We adopt the numerical method dubbed as the "excision technique" to solve the Eqs. (3.15) to (3.17), which provides a numerically feasible way to deal with the radial range beyond the event horizon, which is physically inaccessible. We refer the reader to Ref.[17, 27, 28] for the details. In this work, we employ Matlab's PDE solver toolbox with an FDTD solver. The computational radial domain is set as $0.5 < \tilde{r} < 110$ and the propagation is computed in the range $0 < \tilde{t} < 110$, where $\tilde{r} = r/\xi$, $\tilde{t} = tc_\infty/\xi$ are dimensionless coordinates. For the outer computational boundary, one has to implement absorbing boundary

conditions or simply ignore it by completing the simulation before the outgoing wave reaches to the outer boundary. The inner computational boundary is set beyond the event horizon. The aforementioned excision technique introduces additional constraint equations at the event horizon that have to be monitored to ensure that no perturbation propagates from beyond the event horizon into the physically relevant part of the computational domain.

The incident perturbative wave is chosen to be

$$\psi_1(0, r) = N \exp \left[-(r - r_0 + c(r)t)^2 / b^2 - i\omega(r - r_0 + c(r)t) / c(r) \right]. \quad (4.1)$$

This defines a cylindrically imploding Gaussian wave, initially centered at r_0 , of width b . In the numerical calculations $r_0 = 50\xi$ and $b = 10\xi$ are used. The initial values of π_1 and γ_1 are calculated by Eq.3.13. It is worth to mention that, the density profile given in Eq.2.7 is based inherently on the scaling by the healing length, ξ . The velocity is scaled by c_∞ ,

$$\vec{v} = -\frac{1}{3\sqrt{3}} \left(\frac{1}{\tilde{r}} + \frac{2}{\tilde{r}^3} \right) \hat{r} + \frac{\sqrt{2}}{\tilde{r}} \hat{\theta} \quad (4.2)$$

The energy of the perturbations is given by

$$E(t) = \int \partial^3 r \frac{1}{2} M \rho \vec{v}^2 = (\hbar^2 / 2M) \int_0^{2\pi} d\phi \int_0^H dz \int_1^{r_{max}} \rho(r) (\nabla \Phi)^2 r dr. \quad (4.3)$$

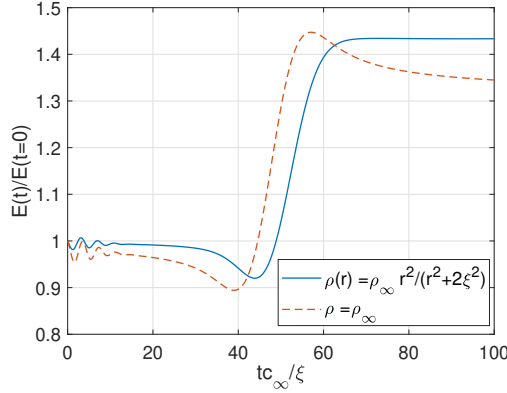


Figure 3: Time evaluation of the energy gain of the wave packet for superradiant case for constant and non-constant density profiles. Wave parameters used are $r_0 = 50\xi$ and $b = 10\xi$ with $\omega = 0.8c_\infty/\xi$

Fig.3 shows the temporal change of the relative energy calculated by the constant background density approximation and by the present formulation. For comparison, the event horizon is set at $r_h = \xi$, same initial perturbative wave is applied in both cases. Nevertheless, the ergosphere and the radial speed differ,

which delays the arrival of the incident perturbation to the event horizon for the non-constant density as seen in the Figure. For the constant background density case, the amplification exhibits an overshooting transient behavior, whereas in the case of the non-constant background density, the amplification saturates monotonically to its final value. Overall, the non-constant background density case predicts a slightly higher ($\sim 8\%$) amplification.

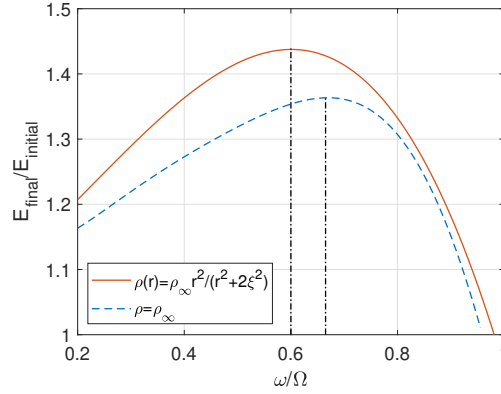


Figure 4: Energy gain difference between constant density and non-constant density approach for $\tilde{\Omega}/5 < \tilde{\omega} < \tilde{\Omega}$. Parameters given in Fig.3

In Figure 4 the spectra of the relative energy for the constant and non-constant background density cases are plotted respectively. Since $\vec{v}_\theta = \vec{\Omega} \times \vec{r}$, the angular frequency of the vortex is equal to

$$\Omega = \frac{B}{r_h^2} = \sqrt{2}c_\infty/\xi \quad (4.4)$$

A subtle but important difference is that, in the constant background density case, Ω appears as an independent and unlimited parameter, whose integer multiples, $m\Omega$, define vortex rotational speed. Of course, $m = 1$ is known to describe a stable vortex. In contrast, the non-constant self-consistent density profile dictates the radial velocity and hence the value of Ω is "built-in" with a particular value that cannot be changed arbitrarily, unless the density profile is modified.

The frequency range of the incident perturbative wave is taken as $0.2 < \omega/\Omega < 1$ since the superradiance is expected for $\omega < m\Omega$, and $m = 1$ for stable vortices. The comparison with constant and non-constant density profiles indicate that in the latter case, the maximum superradiance is obtained at a slightly lower frequency.

5 The spectral analysis of superradiance

We begin by writing the Klein-Gordon equation (Eq.3.12) with a formal solution of the form:

$$\Phi_1 = R(r)e^{i(m\theta - \omega t)} \quad (5.1)$$

$$\frac{\partial^2 R(r)}{\partial^2 r} + P(r)\frac{\partial R(r)}{\partial r} + Q(r)R(r) = 0, \quad (5.2)$$

where

$$P(r) = \left(-2i\omega v_r + \frac{2imv_r v_\theta}{r} - \frac{v_\theta^2 + v_r^2 - c^2}{r} - \frac{c^2}{\rho} \frac{\partial \rho}{\partial r} + \frac{\partial}{\partial r} \left(v_r^2 + \frac{v_\theta^2}{2} \right) \right) \frac{1}{v_r^2 - c^2}, \quad (5.3)$$

$$Q(r) = \left(-\omega^2 + \frac{2m\omega v_\theta}{r} - m^2 \left(\frac{-c^2 + v_\theta^2}{r^2} \right) - i\omega \left(\frac{1}{r} \frac{\partial(rv_r)}{\partial r} \right) - \frac{imv_\theta v_r}{r^2} + \frac{imv_\theta}{r} \frac{\partial v_r}{\partial r} \right) \frac{1}{v_r^2 - c^2}, \quad (5.4)$$

According to the coefficient of dr^2 in the line element (Eq.3.22), we define tortoise coordinate transformation $r \rightarrow r_*$, which maps the radial range $r \in (r_h, \infty)$ unto $r_* \in (-\infty, \infty)$

$$\Delta = \frac{dr_*}{dr} = \left(1 - \frac{v_r^2}{c^2} \right)^{-1} \quad (5.5)$$

Next, the radial part of the solution is expressed in a product form $R(r) = H(r_*)Z(r)$, where the functions respectively satisfy the following differential equations

$$\frac{\partial Z(r)}{\partial r} + M(r)Z(r) = 0, \quad (5.6)$$

$$\frac{\partial^2 H(r_*)}{\partial r_*^2} + V(r)H(r_*) = 0; \quad (5.7)$$

The solution of Eq.5.6 is given by Eq.5.6 gives

$$Z(r) = C \exp \left(- \int M(r) dr \right) \quad (5.8)$$

$$= C \left(\frac{r^2 + 2\xi^2}{r^3} \right)^{1/2} \exp \left(i \int h(r) dr \right) \quad (5.9)$$

where

$$h(r) = \frac{v_r(v_\theta - r\omega)}{r(v_r^2 - c^2)}, \quad (5.10)$$

C is an arbitrary constant. We note that all velocity terms in Eq.5.10 are functions of the radial coordinate. Equation 5.7 is in the form of a time-independent Schrodinger equation with

$$V(r) = \frac{1}{\Delta^2} \left(\frac{\partial M}{\partial r} + M^2 + PM + Q \right) \quad (5.11)$$

$$M(r) = - \left(\frac{P}{2} + \frac{1}{2\Delta} \frac{\partial \Delta}{\partial r} \right) \quad (5.12)$$

Where the $V(r)$ reads explicitly

$$\begin{aligned} V(r) = & \left(\frac{\omega}{c} - \frac{mv_\theta}{rc} \right)^2 + \frac{(v_r^2 - c^2) v_r^2 (5r^4 + 76r^2\xi^2 + 180\xi^4)}{4c^4r^2(r^2 + 2\xi^2)^2} \\ & + \frac{(v_r^2 - c^2) \left(4m^2 (r^2 + 2\xi^2)^2 - r^4 - 20r^2\xi^2 + 12\xi^4 \right)}{4c^2r^2 (r^2 + 2\xi^2)^2} \end{aligned} \quad (5.13)$$

The first term is clearly a function of the energy of the incident perturbative wave while the last two terms depend on r only. We note that $v_r(r)$ and $c(r)$ can be expressed in terms of the event horizon (through Eq.3.23) and the background density profile. Indeed, one can express $V(r)$ in dimensionless coordinates as

$$V(\tilde{r}, \tilde{\omega}) = E(\tilde{r}, \tilde{\omega}) + V_1(\tilde{r}) \quad (5.14)$$

$$E(\tilde{r}, \tilde{\omega}) = \frac{1}{\xi^2} \left(\frac{\tilde{r}^2 + 2}{\tilde{r}^2} \left(\tilde{\omega} - \frac{m\tilde{\Omega}}{\tilde{r}^2} \right)^2 \right) \quad (5.15)$$

$$\begin{aligned} V_1(\tilde{r}) = & - \left((-27\tilde{r}^8 + \tilde{r}^6 + 6\tilde{r}^4 + 12\tilde{r}^2 + 8) (2768\tilde{r}^2 + 2032\tilde{r}^4 + 696\tilde{r}^6 + 430\tilde{r}^8 \right. \\ & \left. - 535\tilde{r}^{10} - 27\tilde{r}^{12} + 108m^2\tilde{r}^8 (\tilde{r}^2 + 2) + 1440) \right) / (2916\xi^2\tilde{r}^{18}(\tilde{r}^2 + 2)^2) \end{aligned} \quad (5.16)$$

Figure 5, panel (a) shows the radial behavior of $V(\tilde{r}_*, \tilde{\omega})$ for $m = 1$ with different values of $\tilde{\omega}$ and panel (b) shows the contributions of the terms to $V(\tilde{r}_*, \tilde{\omega})$ as defined above at fixed $\tilde{\omega} = 0.87$. Figure 6 shows the same quantities for $m = 0$. The comparison provides features that correlate with the existence and the maximum of the superradiance: The ordering of the $\tilde{\omega}$ -level curves at either end of the range are reversed for the superradiant case (Fig.5(a)) whereas they are simply shifted for the $m = 0$ case. Interestingly, the maximum superradiance is achieved when the asymptotic values of $V(\tilde{r}_* \rightarrow +\infty) = V(\tilde{r}_* \rightarrow -\infty)$, i.e. the value of the energy-potential function at the event horizon matches the far-field value. Since $V_1(\tilde{r}_* \rightarrow +\infty) = 0$ as shown in Fig.5 (b), the maximum superradiance is in fact controlled by the $E(\tilde{r}_*, \tilde{\omega})$ which makes a dip between the event horizon and the ergosphere. In contrast, in the non-superradiant ($m = 0$) case, $E(\tilde{r}_*, \tilde{\omega})$ is a monotonically increasing function from its asymptote towards the event horizon.

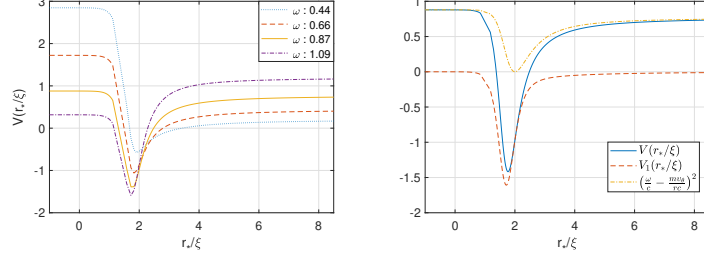


Figure 5: The radial behavior of $V(\tilde{r}_*, \tilde{\omega})$ for $\tilde{\omega} = 0.44, 0.66, 0.87, 1.09$, and behaviors of $E(\tilde{r}, \tilde{\omega})$, $V_1(\tilde{r})$ at fixed $\tilde{\omega} = 0.87$ for $m = 1$

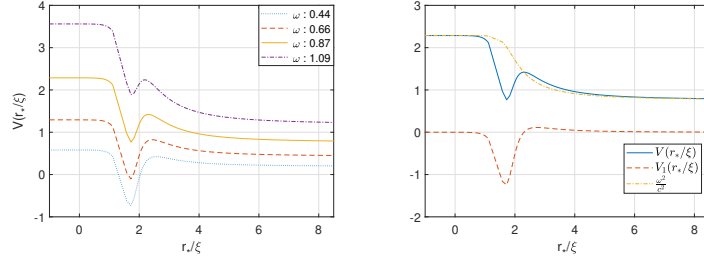


Figure 6: The radial behavior of $V(\tilde{r}_*, \tilde{\omega})$ for $\tilde{\omega} = 0.44, 0.66, 0.87, 1.09$, and behaviors of $E(\tilde{r}, \tilde{\omega})$, $V_1(\tilde{r})$ at fixed $\tilde{\omega} = 0.87$ for $m = 0$.

Returning to the perturbative wave (the massless scalar field in Eq.5.1) we have

$$\Phi_1 = \left(\frac{r^2 + 2\xi^2}{r^3} \right)^{1/2} H(r_*) e^{i(m\theta - \omega t)} e^{i\tilde{h}(r)}. \quad (5.17)$$

Near the event horizon and at $r \rightarrow +\infty$, the solution of Eq.5.7 reduces asymptotically to harmonic solutions

$$H(r_*) = e^{i\frac{\omega}{c_\infty} r_*} + \mathcal{R} e^{-i\frac{\omega}{c_\infty} r_*}, r^* \rightarrow +\infty \quad (5.18)$$

$$H(r_*) = \mathcal{T} e^{-\frac{i}{c(r_h)} \left(\omega - \frac{m v_\phi(r_h)}{r_h} \right) r^*}, r^* \rightarrow -\infty. \quad (5.19)$$

Which introduces complex transmission amplitude through r_h and a complex reflection amplitude at $r \rightarrow \infty$ (of an outgoing wave) for a perturbative wave of unit amplitude incident to the vortex. There are two linearly independent (complex conjugate) solutions whose Wronskian is constant everywhere. Using the rotational speed of the vortex Ω , the relation between the reflection and transmission coefficients can be expressed as

$$1 - |R|^2 = \sqrt{3} \left(\frac{\omega - m\Omega}{\omega} \right) |T^2|, \quad (5.20)$$

Solving Eq.5.5 and Eq.5.7, the reflection coefficient $|\mathcal{R}|^2$ can be calculated through the Fourier components of the asymptotic far field solutions. Figure 7 shows the spectra of $|\mathcal{R}|^2$ for constant and non-constant density approximations, which differ in all but the $\omega/\Omega \cong 1$ limit. Figure 7 shows the spectral comparison of the reflection coefficient calculated with constant and non-constant background density profiles, respectively. In all but the high frequency part of the spectrum, the reflection coefficient differs substantially, for which higher amplification is found for the non-constant density case.

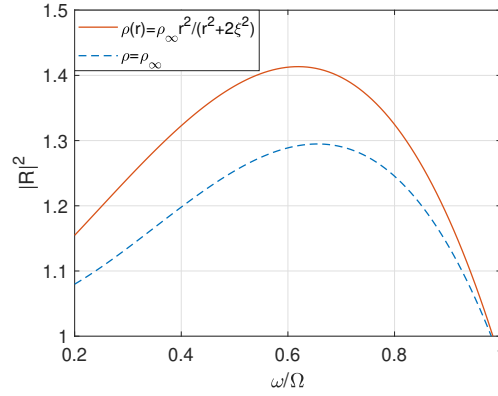


Figure 7: $|R|^2$ is calculated for superradiant case with $\tilde{\Omega} = \sqrt{2}$ in constant and non-constant density profiles.

6 Discussion

In this work, the amplified scattering of axisymmetric acoustic perturbations from the vortex state of a BEC are studied with a self-consistent background density profile. The density profile and a characteristic length scale (e.g. the healing length) used in the formulation inherently defines the vortex parameters (event horizon, angular speed). This is a prominent feature not available in the constant background density approximation. In fact, under constant background density, the rotational speed of the vortex stands as an independent parameter that can be changed arbitrarily. When the frequency of the incident perturbative wave is close to that of the vortex rotational speed $\omega \approx \Omega$ the constant background density agrees well with the result of the non-constant density. At lower frequencies, the non-constant density provides higher superradiance. A prospective study is to extend the present formulation to bound BEC subject to a confining potential, coaxial with the vortex. The "spilling" of

the superradiance from the asymptotic edge of the confining potential would be an interesting feature to investigate.

References

- [1] W. G. Unruh. Experimental black-hole evaporation? *Phys. Rev. Lett.*, 46:1351–1353, May 1981.
- [2] Carlos Barceló, Stefano Liberati, and Matt Visser. Analogue gravity. *Living reviews in relativity*, 14(1):3, 2011.
- [3] Silke Weinfurtner, Edmund W. Tedford, Matthew C. J. Penrice, William G. Unruh, and Gregory A. Lawrence. Measurement of stimulated hawking emission in an analogue system. *Phys. Rev. Lett.*, 106:021302, Jan 2011.
- [4] Oren Lahav, Amir Itah, Alex Blumkin, Carmit Gordon, Shahar Rinott, Alona Zayats, and Jeff Steinhauer. Realization of a sonic black hole analog in a bose-einstein condensate. *Phys. Rev. Lett.*, 105:240401, Dec 2010.
- [5] M. Elazar, V. Fleurov, and S. Bar-Ad. All-optical event horizon in an optical analog of a laval nozzle. *Phys. Rev. A*, 86:063821, Dec 2012.
- [6] Thomas G Philbin, Chris Kuklewicz, Scott Robertson, Stephen Hill, Friedrich König, and Ulf Leonhardt. Fiber-optical analog of the event horizon. *Science*, 319(5868):1367–1370, 2008.
- [7] Jeff Steinhauer. Observation of self-amplifying hawking radiation in an analogue black-hole laser. *Nature Physics*, 10(11):864, 2014.
- [8] Jeff Steinhauer. Observation of quantum hawking radiation and its entanglement in an analogue black hole. *Nature Physics*, 12(10):959, 2016.
- [9] Neil N. Carlson. A topological defect model of superfluid vortices. *Physica D: Nonlinear Phenomena*, 98(1):183 – 200, 1996.
- [10] Alexander L Fetter and Anatoly A Svidzinsky. Vortices in a trapped dilute bose-einstein condensate. *Journal of Physics: Condensed Matter*, 13(12):R135, 2001.
- [11] Jean Macher and Renaud Parentani. Black-hole radiation in Bose-Einstein condensates. *Physical Review A*, 80(4):043601, 2009.
- [12] Luis Javier Garay, JR Anglin, J Ignacio Cirac, and P Zoller. Sonic black holes in dilute bose-einstein condensates. *Physical Review A*, 63(2):023611, 2001.
- [13] Soumen Basak and Parthasarathi Majumdar. Superresonance from a rotating acoustic black hole. *Classical and Quantum Gravity*, 20(18):3907, 2003.

- [14] Theo Torres, Sam Patrick, Antonin Coutant, Maurício Richartz, Edmund W Tedford, and Silke Weinfurtner. Rotational superradiant scattering in a vortex flow. *Nature Physics*, 2017.
- [15] Carlos Barcelo, Stefano Liberati, and Matt Visser. Analogue gravity from Bose-Einstein condensates. *Classical and Quantum Gravity*, 18(6):1137, 2001.
- [16] Mark A Scheel, Adrienne L Erickcek, Lior M Burko, Lawrence E Kidder, Harald P Pfeiffer, and Saul A Teukolsky. 3d simulations of linearized scalar fields in kerr spacetime. *Physical Review D*, 69(10):104006, 2004.
- [17] C Cherubini, F Federici, S Succi, and MP Tosi. Excised acoustic black holes: The scattering problem in the time domain. *Physical Review D*, 72(8):084016, 2005.
- [18] F Federici, C Cherubini, S Succi, and MP Tosi. Superradiance from hydrodynamic vortices: A numerical study. *Physical Review A*, 73(3):033604, 2006.
- [19] Christopher J Pethick and Henrik Smith. *Bose-Einstein Condensation in Dilute Gases*. Cambridge University Press, 2002.
- [20] Anton S Desyatnikov, Lluís Torner, and Yuri S Kivshar. Optical vortices and vortex solitons. *arXiv preprint nlin/0501026*, 2005.
- [21] Yanzhi Zhang, Weizhu Bao, and Qiang Du. Numerical simulation of vortex dynamics in ginzburg-landau-schrödinger equation. *European Journal of Applied Mathematics*, 18(5):607–630, 2007.
- [22] T R Slatyer and C M Savage. Superradiant scattering from a hydrodynamic vortex. *Classical and Quantum Gravity*, 22(19):3833, 2005.
- [23] Soumen Basak and Parthasarathi Majumdar. Reflection coefficient for superresonant scattering. *Classical and Quantum Gravity*, 20(13):2929, 2003.
- [24] Matt Visser. Acoustic black holes: horizons, ergospheres and hawking radiation. *Classical and Quantum Gravity*, 15(6):1767, 1998.
- [25] Franco Dalfovo, Stefano Giorgini, Lev P Pitaevskii, and Sandro Stringari. Theory of bose-einstein condensation in trapped gases. *Reviews of Modern Physics*, 71(3):463, 1999.
- [26] Mike H Anderson, Jason R Ensher, Michael R Matthews, Carl E Wieman, and Eric A Cornell. Observation of bose-einstein condensation in a dilute atomic vapor. *science*, 269(5221):198–201, 1995.
- [27] Miguel Alcubierre and Bernd Brügmann. Simple excision of a black hole in $3 + 1$ numerical relativity. *Phys. Rev. D*, 63:104006, Apr 2001.

- [28] Betül Demirkaya, Tekin Dereli, and Kaan Güven. Analog black holes and energy extraction by super-radiance from bose einstein condensates (bec) with constant density. *arXiv preprint arXiv:1806.02139*, 2018.